ISSN 1674-1056
http://cpb.iphy.ac.cn
http://iopscience.iop.org/cpb
中国物理 B
Chinese Physics
中国物理
Chinese Physics B

Radiation from finite cylindrical shell with irregular-shaped acoustic enclosure

De-Sen Yang(杨德森), Rui Zhang(张睿), Sheng-Guo Shi(时胜国)
Citation: Chin. Phys. B . 2018, 27(10): 104301. **doi:** 10.1088/1674-1056/27/10/104301

Journal homepage: http://cpb.iphy.ac.cn; http://iopscience.iop.org/cpb

What follows is a list of articles you may be interested in

Propagation of acoustic waves in a fluid-filled pipe with periodic elastic Helmholtz resonators

Dian-Long Yu(郁殿龙), Hui-Jie Shen(沈惠杰), Jiang-Wei Liu(刘江伟), Jian-Fei Yin(尹剑飞), Zhen-Fang Zhang(张振方), Ji-Hong Wen(温激鸿)
Chin. Phys. B . 2018, 27(6): 064301. **doi:** 10.1088/1674-1056/27/6/064301

Simultaneous detection of the acoustic-field aberration and Doppler shift in forward acoustic scattering

Chuan-Lin He(何传林), Kun-De Yang(杨坤德), Yuan-Liang Ma(马远良), Bo Lei(雷波)
Chin. Phys. B . 2017, 26(1): 014301. **doi:** 10.1088/1674-1056/26/1/014301

Analysis of underwater decoupling properties of a locally resonant acoustic metamaterial coating

Ling-Zhi Huang(黄凌志), Yong Xiao(肖勇), Ji-Hong Wen(温激鸿), Hai-Bin Yang(杨海滨), Xi-Sen Wen(温熙森)
Chin. Phys. B . 2016, 25(2): 024302. **doi:** 10.1088/1674-1056/25/2/024302

Underwater asymmetric acoustic transmission structure using the medium with gradient change of impedance

Bo Hu(胡博), Jie Shi(时洁), Sheng-Guo Shi(时胜国), Yu Sun(孙玉), Zhong-Rui Zhu(朱中锐)
Chin. Phys. B . 2016, 25(2): 024305. **doi:** 10.1088/1674-1056/25/2/024305

Acoustic radiation from the submerged circular cylindrical shell treated with active constrained layer damping

Yuan Li-Yun, Xiang Yu, Lu Jing, Jiang Hong-Hua
Chin. Phys. B . 2015, 24(12): 124301. **doi:** 10.1088/1674-1056/24/12/124301

Radiation from finite cylindrical shell with irregular-shaped acoustic enclosure*

De-Sen Yang(杨德森)[1,2], Rui Zhang(张睿)[2], and Sheng-Guo Shi(时胜国)[1,2,†]

[1] *Acoustic Science and Technology Laboratory, Harbin Engineering University, Harbin* 150001, *China*
[2] *College of Underwater Acoustic Engineering, Harbin Engineering University, Harbin* 150001, *China*

(Received 15 March 2018; revised manuscript received 21 July 2018; published online 10 September 2018)

In practical situations, large machinery is usually placed in an underwater vessel and changes the acoustic enclosure shape into an irregular one. The existence of machinery causes the difficulties in expressing sound transmission and radiation analytically. In this study, the sound radiation of a cylindrical shell excited by an internal acoustic source is modeled and analyzed. The cylindrical shell contains a machine modeled as a rectangular object, which is attached to a shell with a spring-mass system. The acoustic field of the cavity is computed by the integro-modal approach. The effect of object size on the coupling between acoustic mode and structural mode is investigated. The relationship between object volume and sound radiation is also studied. Numerical results show that the existence of objects inside vessels leads to a more effective coupling between the structure and acoustic enclosure than the existence of no objects in a regular-shaped cavity (i.e. empty vessel).

Keywords: irregular-shaped enclosure, sound radiation, integro-modal approach

PACS: 43.30.+m, 43.40.+s, 43.20.Tb **DOI:** 10.1088/1674-1056/27/10/104301

1. Introduction

Water-loaded cylindrical enclosures are widely used as simple examples for demonstrating the acoustic characteristics of underwater vessels. Enclosures are usually constructed with relatively thin materials, and an important component of sound radiation is related to airborne noise inside these vehicles. Due to the existence of internal structures and machinery inside the vehicle, the enclosure is changed from a regular enclosure into an irregular-shaped enclosure. Subsequently, the characteristics of sound radiation from the vehicle become very complex. The analyzing of the noise transmitted through the enclosure walls is often problematic. Dowell[1] and Lyon[2] presented early models on vibration and cavity-backed plates. Narayanan[3,4] investigated sound transmission properties through a sandwiched panel and into a rectangular enclosure. Interior noise in an enclosure could be decomposed using an orthogonal expansion. Dowell[5] presented a comprehensive theoretical model based on the modal expansion theory and Green's theorem to analyze the sound transmission characteristics of a panel with structural-acoustic coupling, then James[6] employed a similar approach for internally excited cylindrical shells. Fuller[7] presented the reasons behind the different transmission losses of a shell wall by analyzing theoretical values and experimental data from a previous research (see Morfey[8]). Further, Lee[9] analyzed the characteristics of sound transmission into a cylindrical shell through theoretical and experimental research.

In contrast to the empty cylindrical shell, the shell with internal structures and added mass seems to be a more realistic model. There is a considerable amount of literature dealing with the effects of rings,[10] rigid discs,[11] anechoic coatings,[12] and bulkheads.[13–15] In ships and submarines, internal structures and machinery are often mounted into hulls by using a type of resilient material that can isolate vibration. Approximately, the resilient material can be regarded as a spring system, and the internal structure as mass attached to it.[16,17] Guo[18] showed that the attachment of the simple spring-mass loading causes significant changes in the acoustic behavior of the shell. Titovich and Norris[19] extended the analysis by considering a cylindrical shell with an internal mass attached by multiple axisymmetrically distributed stiffeners.

In previous work, internal machinery was often regarded as an internal spring-mass system without considering its volume effect. In fact, the inner space of a shell becomes irregular because of the existence of machines, and the acoustic modes of the shell become difficult to express analytically. Missaoui and Cheng[20,21] proposed the combined integro-modal approach to handle irregular-shaped cavities, in which the interior acoustic field is simplified as either a model for regular sub-cavities or the boundary cavities with irregular-shaped boundaries. Despite the findings that geometric deformities of the cavity[22] or the internal structure inside an acoustic enclosure[23,24] can affect the structural-acoustic coupling be-

*Project supported by the National Natural Science Foundation of China (Grant No. 61601149) and the Program for Changjiang Scholars and Innovative Research Team in University of Ministry of Education of China (Grant No. IRT_16R17).

†Corresponding author. E-mail: shishengguo@hrbeu.edu.cn

© 2018 Chinese Physical Society and IOP Publishing Ltd

tween shells and their interior acoustic field, studies on the influence of machinery volume occupation on structural acoustic coupling remain limited. In practice, a machine has a finite size and, in most cases, occupies a large part of the vehicle interior space. Consequently, the existence of internal machineries affects the acoustic field inside the shell, thereby changing the vibration and sound radiation.

The purpose of the present study is to investigate the possible effects of machinery volume on the interior acoustic field and sound radiation of a submerged cylindrical shell excited by an internal monopole acoustic source.

The present work is to extend the previous model[25] by considering a finite shell containing a finite-sized mechanical machine modelled as a rectangular object. The integro-modal approach is adopted to deal with the irregular-shaped acoustic enclosure caused by the machine. Then a complex vibro-acoustic system is performed to discuss phenomena on the shell with an irregular-shaped acoustic enclosure. Although numerical methods are general and successfully used in the past to analyze irregular-shaped cavities and other models in the low-frequency range, it is clear that physical models establishment is necessary for parametric studies.[26] The rest of the present paper is organized as follows. The mathematical formulation is described in Section 2. In Section 3, numerical results are presented and discussed. First, the coupling characteristics of a cylindrical shell with irregular-shaped cavity are analyzed and compared with those of a regular shell. Second, based on the tendency curves, the relationship between machine size and structural vibration is determined. Finally, the effect of machinery volume on sound radiation and far-field directivity of the shell are examined.

2. Governing equations

A finite thin cylindrical shell with thickness h, radius R, length L, and in-vacuo bulk mass density ρ_s is considered for analysis. Considering a single cylindrical section, the shell bulkheads are simplified into two rigid end plates (to form a finite cylinder for the internal acoustic field) attached to two semi-infinite rigid baffles to prevent the sound from transmitting between compartments.[27,28] A mechanical machine is modeled as a rectangular box with a square cross section and a slightly shorter length than the shell to avoid end-plate influence. The box with a rigid boundary and mass M is attached to the inner surface of the shell by continuous springs, each with stiffness κ (unit of force per unit area). The cylindrical coordinate system used for analysis is shown in Fig. 1(a). The cross-section of the shell with an interior monopole source is illustrated in Fig. 1(b).

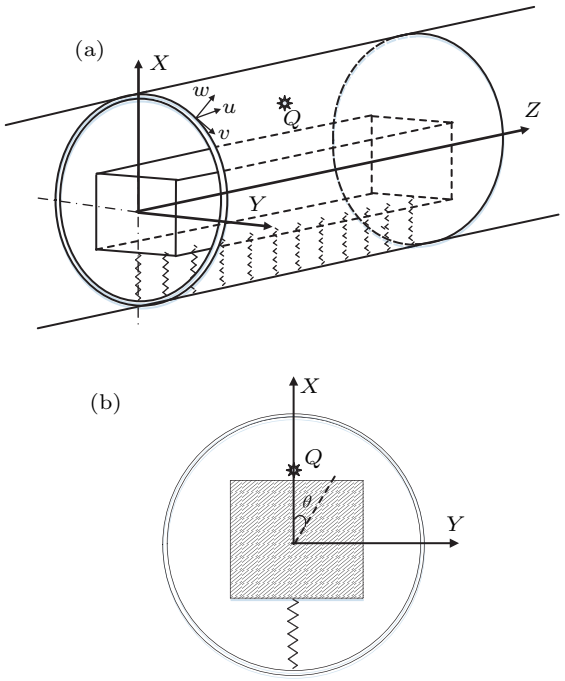


Fig. 1. Geometry and coordinate system of a cylindrical shell, showing (a) finite cylindrical shell with semi-infinite baffles and (b) cross-section of shell with monopole source.

2.1. Shell displacements

Consider a harmonic motion, the radial displacement of the shell, w, is coupled to the other two displacement components, namely, u in the axial direction and v in the circumferential direction, through dynamic equations for shell vibrations. Donnell's thin shell equation[29] is used to describe the equations of motion of the cylindrical shell. The equation is written as follows:

$$[\boldsymbol{L}_{ij}]\{\, u \;\; v \;\; w \,\}^{\mathrm{T}} = \frac{1-\sigma^2}{Eh}\{\boldsymbol{p}_{\mathrm{f}}^{\mathrm{T}} - \boldsymbol{F}_{\mathrm{s}}^{\mathrm{T}} - \boldsymbol{p}_{\mathrm{e}}^{\mathrm{T}}\}, \tag{1}$$

where $\boldsymbol{L}_{ij}$ represent the differential operator of Donnell's shell equation. $\boldsymbol{F}_{\mathrm{s}}^{\mathrm{T}}$ represents the stress of the spring-mass system on the inner surface of the shell. $\boldsymbol{p}_{\mathrm{f}}^{\mathrm{T}}$ and $\boldsymbol{p}_{\mathrm{e}}^{\mathrm{T}}$ are the sound pressure on the interior and exterior surface of the cylindrical shell, respectively. E is Young's modulus. Poisson's ratio is denoted by σ. Since the problem is linear, the time dependence of all quantities can be assumed to be $\exp(-\mathrm{i}\omega t)$. This factor is suppressed throughout.

The displacement function of the shell is simply supported on its end, which is satisfied with boundary conditions, can be expanded using modes as follows:

$$\begin{Bmatrix} u(\theta,z) \\ v(\theta,z) \\ w(\theta,z) \end{Bmatrix} = \sum_{\alpha=0}^{1}\sum_{m=1}^{\infty}\sum_{n=0}^{\infty} \begin{Bmatrix} U_{\alpha mn}\cos(n\theta-\alpha\pi/2)\cos(m\pi z/L) \\ V_{\alpha mn}\sin(n\theta-\alpha\pi/2)\sin(m\pi z/L) \\ W_{\alpha mn}\cos(n\theta-\alpha\pi/2)\sin(m\pi z/L) \end{Bmatrix}, \tag{2}$$

where $U_{\alpha mn}$, $V_{\alpha mn}$, and $W_{\alpha mn}$ are the modal vectors of the corresponding simply supported shell with n, and m being the circumferential and longitudinal order, respectively, and $\alpha = 0$ (or 1) means the symmetric (or antisymmetric) mode.

The pressure field outside of the shell is written as[30–32]

$$p_{\mathrm{e}}(r,\theta,z) = \frac{\rho_1\omega^2}{k_{\mathrm{e}}^2 L}\sum_{\alpha,m,n} m\sin\left(n\theta+\frac{\alpha\pi}{2}\right) \times \int_0^{+\infty} W_{\alpha mn}\frac{G_m(\lambda)}{\sqrt{1-\lambda^2}}\frac{S_m(\lambda)}{\left(\frac{m\pi}{k_{\mathrm{e}}L}\right)^2-\lambda^2}\mathrm{d}\lambda, \quad (3)$$

where

$$G_m(\lambda) = \begin{cases} \dfrac{\mathrm{H}_n\left(k_{\mathrm{e}}\sqrt{1-\lambda^2}r\right)}{\mathrm{H}_n'\left(k_{\mathrm{e}}\sqrt{1-\lambda^2}R\right)}, & \lambda \le 1, \\ \dfrac{\mathrm{K}_n\left(k_{\mathrm{e}}\sqrt{1-\lambda^2}r\right)}{\mathrm{K}_n'\left(k_{\mathrm{e}}\sqrt{1-\lambda^2}R\right)}, & \lambda > 1, \end{cases} \quad (4)$$

$$S_m(\lambda) = \frac{1}{2}\mathrm{e}^{\mathrm{i}k_{\mathrm{e}}\lambda z}\left[1-(-1)^m\mathrm{e}^{-\mathrm{i}k_{\mathrm{e}}\lambda L}\right], \quad (5)$$

where $k_{\mathrm{e}} = \omega/c_1$ is the wavenumber in the fluid outside the shell; ρ_1 is the density of water; $\mathrm{H}_n(\cdot)$ and $\mathrm{K}_n(\cdot)$ are the n-th order Hankel function and modified Hankel function of the first kind, respectively; $\mathrm{H}_n'(\cdot)$ and $\mathrm{K}_n'(\cdot)$ indicate the differentiation of Hankel function and modified Hankel function with respect to the argument.

The spring-mass system is connected to the shell as shown in Fig. 1. The springs are assumed to be evenly distributed. The derivation of the linearized equations of motion for the internal mass and the resulting radial force on the shell are described in Ref. [19]. More detailed derivation can be found in Ref. [16]. The displacement of the finite sized mass associated with its rotation is of the second order and vanishes in the equations, which means that the shell does not experience tangential force and only the translating degrees of freedom of the mass contribute to the radial force on the shell.

$$F_{\mathrm{s}}(\theta,z) = -\frac{\kappa}{R}\left(\frac{\tau^2}{\tau^2-1}\right)w(\theta,z)\,\delta(\theta-\theta_{\mathrm{s}}), \quad (6)$$

where $\delta(\cdot)$ is the Dirac delta function and

$$\tau^2 = \omega^2/\omega_{\mathrm{sp}}^2 = M\omega^2/\kappa \quad (7)$$

with ω_{sp} being the natural frequency of the oscillator.

2.2. Interior sound field

With the consideration of the machine size, the acoustic enclosure of the shell becomes irregular. For the irregular-shaped enclosure, the internal pressure is handled by using the integro-modal approach.[20,21] In the method the whole cavity is discretized into a series of sub-cavities, whose acoustic pressure is simplified as either over a modal basis of regular sub-cavities or over that of the bounding cavities in the case of irregular-shaped boundaries. In the present paper a point source item is introduced into the integro-modal formulation to analyze the influence of the internal object.

Green's theorem together with the Helmholtz equation is used for describing the interior sound pressure

$$p_{\mathrm{f}}(r) = \int_{S_{\mathrm{c}}}\left[\frac{\partial p_{\mathrm{f}}(r')}{\partial \boldsymbol{n}}G(r,r') - p_{\mathrm{f}}(r')\frac{\partial G(r,r')}{\partial \boldsymbol{n}}\right]\mathrm{d}s + \int_V \Im(r_{\mathrm{s}},\omega)\,G(r,r_{\mathrm{s}})\,\mathrm{d}v, \quad (8)$$

where p_{f} is the interior sound pressure; $\boldsymbol{n}$ is the outward normal vector of the boundary surface S_{c} of the enclosure with volume V; $\Im(r_{\mathrm{s}},\omega)$ is the function of source distribution, evaluated r_{s} at inside V; and $G(r,r')$ is Green's function corresponding to a transfer function obtained between an observation point (r) and the point (r').

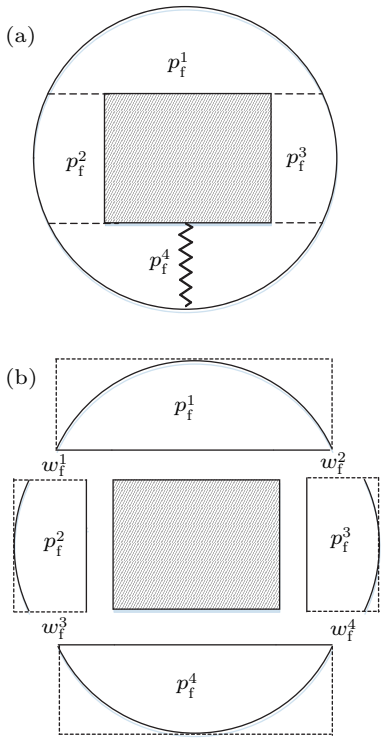


Fig. 2. Discretization procedure using the integro-modal approach, showing (a) the real cavity and (b) four decomposed sub-cavities.

Considering the weak contribution of internal object motion in the internal acoustic field, the boundary condition of the object is simplified into being rigid. The equations for the boundary conditions at the walls of the cavity can be written as

$$\partial p_{\mathrm{f}}/\partial z = 0, \quad z = 0, \quad z = L, \quad (9)$$

$$\partial p_{\mathrm{f}}/\partial \boldsymbol{n} = \rho_2\omega^2 w, \quad \boldsymbol{n} \in S_{\mathrm{s}}, \quad (10)$$

$$\partial p_{\mathrm{f}}/\partial \boldsymbol{n} = 0, \quad \boldsymbol{n} \in S_{\mathrm{b}}, \quad (11)$$

where S_{s} is the inner surface of the cylindrical shell. The surface of the rectangular box is denoted by S_{b}.

The internal pressure is decomposed using an orthogonal expansion in terms of the rigid-walled acoustic modes of rectangular cavities as shown in Fig. 2:

$$p_{\mathrm{f}}^{k}=\rho_2 c_2^2\sum_{\tilde{n}}\frac{a_{\tilde{n}}^{k}}{\Lambda_{\tilde{n}}^{k}}\phi_{\tilde{n}}^{k}(r),\quad 1\le k\le 4, \tag{12}$$

where $\rho_2 c_2$ is the specific acoustic resistance of the interior fluid, $a_{\tilde{n}}^{k}$ is the modal pressure amplitudes to be determined, $\phi_{\tilde{n}}^{k}(r)$ the corresponding mode shape which satisfies the Neumann boundary, and $\Lambda_{\tilde{n}}^{k}=\left(1/V^{k}\right)\int_{V^{k}}\left[\phi_{\tilde{n}}^{k}(r)\right]^{2}\mathrm{d}v$ is the generalized acoustic mass. For the three-dimensional (3D) problem, there are three indices (n_x, n_y, n_z) corresponding to the different orthogonal directions for each sub-cavity mode $(\tilde{n})$. For the present situation, a cosine function can be used for the sub-cavity mode in the form of $\phi_{\tilde{n}}^{k}(r)=\cos\left(n_x\pi x/L_x^{k}\right)\cos\left(n_y\pi y/L_y^{k}\right)\cos\left(n_z\pi z/L_z^{k}\right)$, where L_x^{k}, L_y^{k}, and L_z^{k} are the edge lengths of each sub-cavity in different directions, respectively.

The transverse displacement of the virtual membranes is also expanded in terms of in-vacuo normal mode shapes $\psi_{\tilde{m}}$ as follows:

$$w_{\mathrm{f}}^{k}=\sum_{\tilde{m}}q_{\tilde{m}}^{k}\psi_{\tilde{m}}^{k}, \tag{13}$$

where $q_{\tilde{m}}^{k}$ are the structural modal amplitudes. Substituting Eqs. (12) and (13) into Eq. (8) gives the linear modal acoustic equation below.

$$\begin{aligned}&\left(\omega_{\tilde{n},k}^2-\omega^2\right)a_{\tilde{n}}^{k}+\frac{c_2^2}{V^{k}}\sum_{\tilde{n}'}\frac{a_{\tilde{n}'}^{k}}{\Lambda_{\tilde{n}'}^{k}}\int\varphi_{\tilde{n}'}^{k}\frac{\partial\varphi_{\tilde{n}}^{k}}{\partial\boldsymbol{n}}\mathrm{d}s\\&=\frac{1}{\rho_2 V^{k}}\int_{V^{k}}\Im(r_{\mathrm{s}},\omega)\varphi_{\tilde{n}}^{k}(r_{\mathrm{s}})\mathrm{d}v\\&\quad+\frac{\omega^2 A_{\mathrm{f}}^{k}}{V^{k}}\sum_{\tilde{m}}q_{\tilde{m}}^{k}L_{\tilde{n}\tilde{m}}^{k,k}+\frac{\omega^2 A_{\mathrm{f}}^{k+1}}{V^{k}}\sum_{\tilde{m}}q_{\tilde{m}}^{k+1}L_{\tilde{n}\tilde{m}}^{k,k+1},\quad k=1,\end{aligned} \tag{14}$$

$$\begin{aligned}&\left(\omega_{\tilde{n},k}^2-\omega^2\right)a_{\tilde{n}}^{k}+\frac{c_2^2}{V^{k}}\sum_{\tilde{n}'}\frac{a_{\tilde{n}'}^{k}}{\Lambda_{\tilde{n}'}^{k}}\int\varphi_{\tilde{n}'}^{k}\frac{\partial\varphi_{\tilde{n}}^{k}}{\partial\boldsymbol{n}}\mathrm{d}s\\&=-\frac{\omega^2 A_{\mathrm{f}}^{k-1}}{V^{k}}\sum_{\tilde{m}}q_{\tilde{m}}^{k-1}L_{\tilde{n}\tilde{m}}^{k,k-1}\\&\quad+\frac{\omega^2 A_{\mathrm{f}}^{k+1}}{V^{k}}\sum_{\tilde{m}}q_{\tilde{m}}^{k+1}L_{\tilde{n}\tilde{m}}^{k,k+1},\quad k=2,3,\end{aligned} \tag{15}$$

$$\begin{aligned}&\left(\omega_{\tilde{n},k}^2-\omega^2\right)a_{\tilde{n}}^{k}+\frac{c_2^2}{V^{k}}\sum_{\tilde{n}'}\frac{a_{\tilde{n}'}^{k}}{\Lambda_{\tilde{n}'}^{k}}\int\varphi_{\tilde{n}'}^{k}\frac{\partial\varphi_{\tilde{n}}^{k}}{\partial\boldsymbol{n}}\mathrm{d}s\\&=-\frac{\omega^2 A_{\mathrm{f}}^{k-1}}{V^{k}}\sum_{\tilde{m}}q_{\tilde{m}}^{k-1}L_{\tilde{n}\tilde{m}}^{k,k-1}\\&\quad-\frac{\omega^2 A_{\mathrm{f}}^{k}}{V^{k}}\sum_{\tilde{m}}q_{\tilde{m}}^{k}L_{\tilde{n}\tilde{m}}^{k,k},\quad k=4,\end{aligned} \tag{16}$$

where A_{f}^{k} is the area of the vibrating surface and $\omega_{\tilde{n},k}$ is the angular resonance frequency of the cavity. The corresponding integrations of pressure functions at the four boundary surfaces are summarized as follows:

$$\text{Surface 1:}\ \sum_{\tilde{n}}\frac{a_{\tilde{n}}^{1}}{\Lambda_{\tilde{n}}^{1}}L_{\tilde{n}\tilde{m}}^{1,1}-\sum_{\tilde{n}}\frac{a_{\tilde{n}}^{2}}{\Lambda_{\tilde{n}}^{2}}L_{\tilde{n}\tilde{m}}^{2,1}=0, \tag{17}$$

$$\text{Surface 2:}\ \sum_{\tilde{n}}\frac{a_{\tilde{n}}^{1}}{\Lambda_{\tilde{n}}^{1}}L_{\tilde{n}\tilde{m}}^{1,2}-\sum_{\tilde{n}}\frac{a_{\tilde{n}}^{3}}{\Lambda_{\tilde{n}}^{3}}L_{\tilde{n}\tilde{m}}^{3,2}=0, \tag{18}$$

$$\text{Surface 3:}\ \sum_{\tilde{n}}\frac{a_{\tilde{n}}^{2}}{\Lambda_{\tilde{n}}^{2}}L_{\tilde{n}\tilde{m}}^{2,3}-\sum_{\tilde{n}}\frac{a_{\tilde{n}}^{4}}{\Lambda_{\tilde{n}}^{4}}L_{\tilde{n}\tilde{m}}^{4,3}=0, \tag{19}$$

$$\text{Surface 4:}\ \sum_{\tilde{n}}\frac{a_{\tilde{n}}^{3}}{\Lambda_{\tilde{n}}^{3}}L_{\tilde{n}\tilde{m}}^{3,4}-\sum_{\tilde{n}}\frac{a_{\tilde{n}}^{4}}{\Lambda_{\tilde{n}}^{4}}L_{\tilde{n}\tilde{m}}^{4,4}=0, \tag{20}$$

where

$$L_{\tilde{n}\tilde{m}}^{i,j}=\frac{1}{A_{\mathrm{f}}^{j}}\int_{\mathrm{s_f^j}}\varphi_{\tilde{n}}^{i}(r)\,\psi_{\tilde{m}}^{j}(r)\,\mathrm{d}s^{j}, \tag{21}$$

with $L_{\tilde{n}\tilde{m}}^{i,j}$ being the modal coupling coefficient between the $\tilde{m}$-th structure mode and the $\tilde{n}$-th cavity mode. This term characterizes the coupling in space between the two modes.

2.3. Global system response

So far, all the structural and acoustic subsystems have been formulated. The final matrix equations based on Eqs. (1) and (15)–(20) can be written as

$$\begin{bmatrix}\boldsymbol{K}_{\mathrm{SS}} & 0 & \boldsymbol{K}_{\mathrm{SF}}\\ 0 & 0 & \boldsymbol{C}_{\mathrm{FF}}\\ \boldsymbol{B}_{\mathrm{FS}} & \boldsymbol{B}_{\mathrm{FM}} & \boldsymbol{A}_{\mathrm{FF}}\end{bmatrix}\begin{Bmatrix}\boldsymbol{U}^{\mathrm{s}}\\ \boldsymbol{U}^{\mathrm{m}}\\ \boldsymbol{P}^{\mathrm{c}}\end{Bmatrix}=\begin{Bmatrix}0\\ 0\\ \boldsymbol{P}^{\mathrm{s}}\end{Bmatrix}, \tag{22}$$

where $\boldsymbol{U}^{\mathrm{s}}$, $\boldsymbol{U}^{\mathrm{m}}$, and $\boldsymbol{P}^{\mathrm{c}}$ are the unknowns related to the structural components, virtual membranes, and acoustical vectors, respectively; $\boldsymbol{K}_{\mathrm{SS}}$ is the dynamic stiffness matrix of the structural system; $\boldsymbol{K}_{\mathrm{SF}}$ is the fluid structure coupling matrix; $\boldsymbol{C}_{\mathrm{FF}}$ is the continuity matrix across virtual membranes; $\boldsymbol{B}_{\mathrm{FS}}$ and $\boldsymbol{B}_{\mathrm{FM}}$ are matrices obtained using various coefficients of the acoustoelastic coupling; $\boldsymbol{A}_{\mathrm{FF}}$ contains the acoustical mass and stiffness matrices; and $\boldsymbol{P}^{\mathrm{s}}$ is the vector related to the airborne source excitation.

3. Numerical analysis

In order to analyze the effect of internal objects on the characteristics of the interior acoustic field and the sound radiation, a finite cylindrical shell is taken for an example. The numerical analysis is performed for the parameter values of the vibro-acoustic system gathered in Table 1.

The internal object, which occupies a volume $V_{\mathrm{b}}(a\times a\times L)$ with rigid boundary, is attached to the inner surface of the shell by continuous springs with stiffness κ. The mass-spring system parameter is chosen as the ratio of internal mass to shell mass $M/2\pi\rho_{\mathrm{s}}hRL=3$, and the spring constant κ is chosen as $\kappa=Mc_1^2/R^2L$. To study the effects of the object volume on the interior and exterior acoustic field, a new parameter β is defined as the ratio of the object volume V_{b} to the empty shell volume $V_{\mathrm{c}}\left(\pi R^2L\right)$. The parameter β varies

by choosing different sizes of rectangular cross-sectional area. Structural damping is introduced by using a complex-valued Young's modulus $E \to E(1-\mathrm{i}\eta)$ where η is the loss factor and its value is set to be 0.01.

Table 1. Physical parameters of vibro-acoustic system.

Steel shell	Young's modulus	$E = 2.1 \times 10^{11}$ N/m^2
	Poisson ratio	$\sigma = 0.3$
	material density	$\rho_s = 7800$ kg/m^3
	radius	$R = 3.5$ m
	length	$L = 9.6$ m
	thickness	$h = 0.028$ m
Interior fluid	material density	$\rho_2 = 1.29$ kg/m^3
	sound speed	$c_2 = 343$ m/s
Exterior fluid	material density	$\rho_1 = 1000$ kg/m^3
	sound speed	$c_1 = 1500$ m/s
Monopole source	source strength	$Q = 4\pi$
	Source position	$(r_0, \theta_0, z_0) = (3R/4, 0, L/2)$

The truncation of the decomposition series is a factor affecting the accuracy of the calculation. Roughly speaking, the $\tilde{m}$-th structure mode and $\tilde{n}$-th cavity mode gradually increase until no noticeable change in the calculated result is observed. The sound pressure level is to be examined at the observation point $(3R/4, 180^\circ, L/2)$ in Fig. 3. It can be seen that the convergence rate depends on the number of decomposition terms. As expected, the truncation of the decomposition terms is a computational restriction on the present solution with the increase of frequency. For the present configuration, the characteristics of interior and exterior sound field below the ring frequency are discussed.

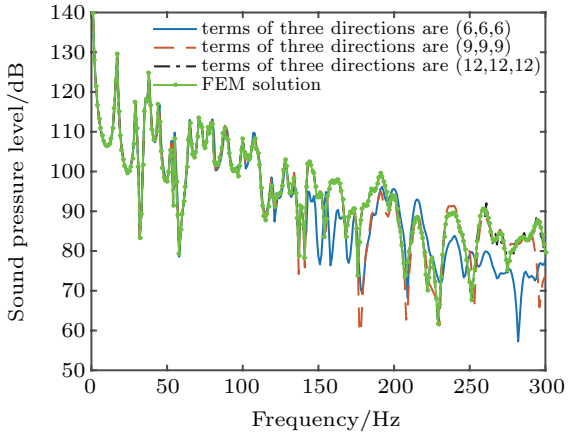


Fig. 3. (color online) Comparisons among curves of sound pressure level versus frequency for different decomposition terms.

Besides, equation (22) can be used to calculate the resonant frequency of the coupled system. The computed results are listed in Table 2 with a comparison with the FEM solution. The errors also depend on the resonant modes and the number of decomposition terms in the expansion. The orders are arranged according to the values of the resonance frequencies. It can be observed that both methods agree well with each other.

Table 2. Resonant frequencies of irregular cavity with $\beta = 0.5$ using different methods.

Mode order	1	2	3	4	5	6	7
FEM solution/Hz	16.591	17.865	24.380	28.066	33.269	35.729	39.393
Present solution/Hz	17.0	18.1	24.2	28.7	33.5	35.7	38.6

3.1. Coupling analysis between structure and enclosure

The coupling analysis between the shell and interior acoustic field due to the variation of β is first investigated. In the case of $\beta = 0$, the enclosure is a regular cylindrical cavity. Due to the perfect symmetry of the system, a structural mode is coupled to an acoustic mode in a very selective manner.[24] For the coupled shell-cavity system, the coupling coefficient between the $\tilde{m}$-th structure mode (p,q) and the $\tilde{n}$-th cavity mode (n_1,n_2,n_3) of the regular cylindrical cavity is

$$\begin{aligned}\zeta_{\tilde{n},\tilde{m}} &= \int_0^L \int_0^{2\pi} \varphi_{\tilde{n}}(R,\theta,z)\sin(q\pi z/L)\cos(p\theta-\alpha\pi/2)\,\mathrm{d}\theta\,\mathrm{d}z \\ &= \sum_{\tilde{n}} J_{n_1}(\chi_{n_1 n_3})\frac{qL[1-(-1)^{q+n_2}]}{\pi(q^2-n_2^2)}\frac{2\pi\delta_{n_1,p}}{\varepsilon_{n_1}}, \quad q \neq n_2, \end{aligned} \tag{23}$$

with p and q being the circumferential and longitudinal order of the structural mode, respectively, and n_1, n_2, and n_3 being the circumferential, longitudinal, and radial order of the acoustic mode, respectively. It is clear that only the odd (even) acoustic modes are coupled to the even (odd) structural modes in the longitudinal direction and both modes have the same circumferential order. In the case of $\beta = 0$, the coupling coefficient no longer exists in the traditional principle. However, the expression for modal force F_{pq} contains a coupling term.

$$\begin{aligned}F_{pq} = \sum_k \iint_{S_k} p_{\mathrm{f}}^k(R,\theta,z)\sin(q\pi z/L) \\ \times\cos(p\theta-\alpha\pi/2)R\,\mathrm{d}\theta\,\mathrm{d}z. \end{aligned} \tag{24}$$

It can be seen that the coefficients of the Fourier series expansion are complicated by the analytical solution. The most convenient method of evaluating the equation is to integrate numerically along the inner surface of the shell. Like the general asymmetric structure, the irregularity of the enclosure can lead to the coupling between each order acoustic mode and structural mode.

3.2. Effect of object volume occupation on interior acoustic field

The existence of the object changes the regular-shaped cavity into an irregular one, and subsequently exerts an influence on the internal acoustic field. An average quadratic pressure is defined inside the enclosure as

$$\left\langle p_{\mathrm{f}}^2(r,\omega)\right\rangle = (1/V_{\mathrm{c}})\int_{V_{\mathrm{c}}} p_{\mathrm{f}}(r,\omega)\cdot[p_{\mathrm{f}}(r,\omega)]^*\,\mathrm{d}v. \quad (25)$$

For the irregular enclosure, the expression turns into a summation form as

$$\left\langle p_{\mathrm{f}}^2(r,\omega)\right\rangle = \frac{1}{V_{\mathrm{c}}-V_{\mathrm{b}}}\sum_k\int_{V_{\mathrm{c}}-V_{\mathrm{b}}} p_{\mathrm{f}}^k(r,\omega)\cdot\left[p_{\mathrm{f}}^k(r,\omega)\right]^*\,\mathrm{d}v. \quad (26)$$

Figure 4 shows the comparisons among the curves of average quadratic pressure versus frequency for different values of β. With the β increasing from 0 to 0.5, the acoustic pressure and resonant peaks deviate gradually from those of its regular case. Clearly, the low-frequency results are more affected by the internal object.

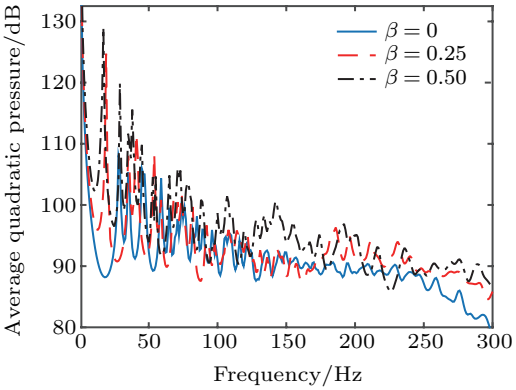


Fig. 4. (color online) Curves of average quadratic pressure versus frequency inside the shell with different values of β.

To discuss the relationship between resonant peak and the object size, figure 5 shows the curve of the resonant peak varying with object size. As is well known, each peak represents one eigenfrequency and one natural mode of the cavity. For a regular rectangular or cylindrical cavity, the eigenfrequency usually becomes higher as the volume of the enclosed space decreases. However, figure 5 shows the opposite trend. Thus it can be seen that the relationship between the eigenfrequency and the spatial scale of the enclosure is not always applicable to the irregular sound cavity. The reason for this phenomenon is that the eigenfrequency is related not only to the geometry size of the cavity, but also to the mode shape of the cavity. Similar cases have also been presented in Ref. [33].

Further analysis is made to identify contributions of the object size to the eigenfrequency. Despite the lack of symmetry in the cross-section area, the irregular cavity can still be expanded among modes with different longitudinal orders. The average quadratic pressures are shown in Figs. 6(a) and 6(b) for the longitudinal order $n_2 = 0$ and 2 below 50 Hz. By comparison, the resonant frequencies of the first few peaks are shifted to the low frequency as the object volume increases in both cases. An exception appears near 35 Hz in Fig. 6(b), because sound fields are homogeneous on the cross section for the isolated peaks.

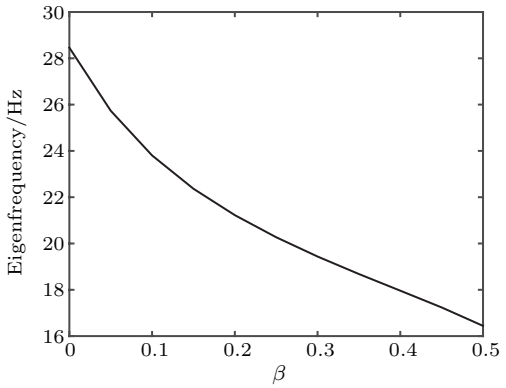


Fig. 5. First resonant peaks with $0 < \beta < 0.5$.

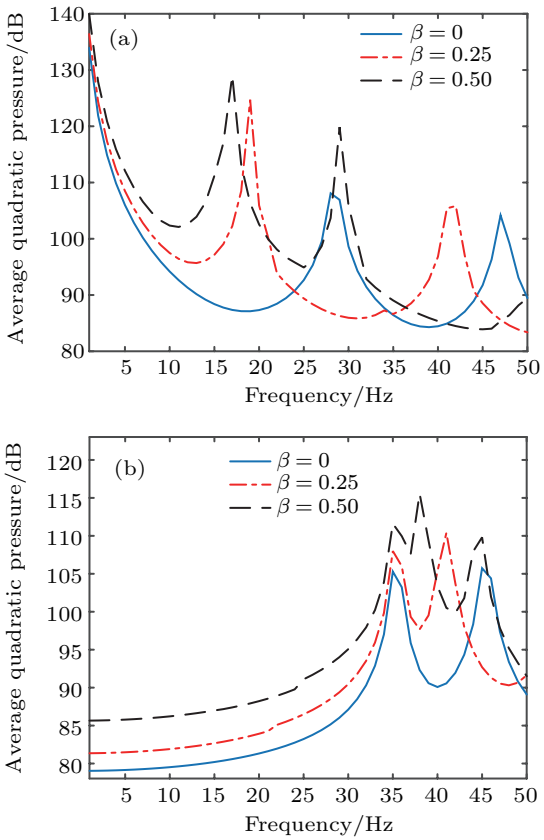


Fig. 6. (color online) Curves of average quadratic pressure versus frequency for different values ofβ with $n_z = 0$ (a) and $n_z = 2$ (b).

For a regular-shaped cavity, equation (24) indicates that the amplitude of the cavity modal distribution is a harmonic function near the inner surface of the cylindrical shell. In the case, each acoustic mode is only coupled to the structural mode with the same circumferential order. For comparison, figure 7 shows the acoustic pressure distributions on the cross section ($z = 0$ and $r = R$) corresponding to the first two eigenfrequencies in Fig. 6(a). The acoustic pressure distributions deviate gradually with the object size increasing, leading to the structural-acoustic coupling among different orders.

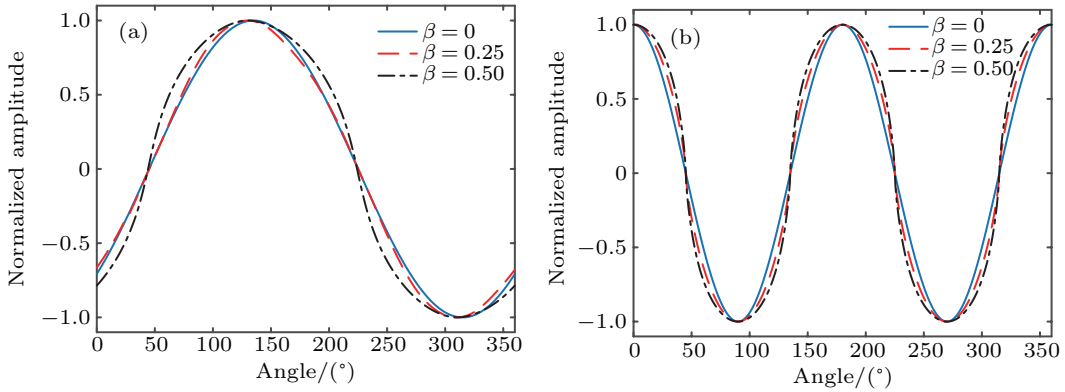


Fig. 7. (color online) Acoustic pressure distributions on the cross section (a) first peaks; (b) second peaks.

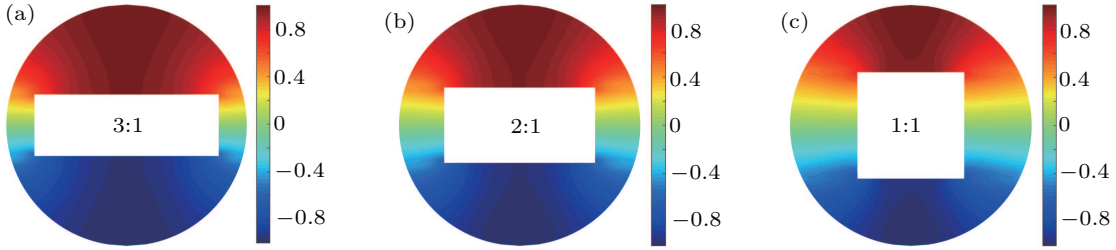


Fig. 8. (color online) Mode shapes for distorted objects with different aspect ratios: (a) 3:1 aspect ratio with resonant frequency 13.3 Hz; (b) 2:1 aspect ratio with resonant frequency 16.2 Hz; (c) 1:1 aspect ratio with resonant frequency 20.2 Hz.

In addition to the volume occupation, the shape of the object is another very practical factor. Figure 8 shows the acoustic pressure distributions inside the cavity ($z = 0$) for a few distorted objects with the same volume and different aspect ratios. The resonant frequencies of the first peaks are shifted with the variation of aspect ratio. There is a similar result for a further increase in aspect ratio.

3.3. Vibration analysis

The effect of the object volume occupation on the internal acoustic field will further cause the vibration response of the shell to change. The average quadratic velocity of the structure is defined as a physical quantity describing the vibration characteristics as follows:

$$\langle V_{\mathrm{s}}^2 \rangle = \frac{\int (V_{\mathrm{s}} \cdot V_{\mathrm{s}}^*)\, \mathrm{d}s}{2\pi RL}, \tag{27}$$

where V_{s} is the vibration velocity of the shell and V_{s}^* is the complex conjugate of V_{s}.

Figure 9 shows the relationship between the object size and the vibration response of the shell. The results indicate that the object volume occupation has an obvious influence on the vibration of the structure in a low-frequency range. Focusing on the low frequency band, it can be found that the distribution of most resonance peaks does not change, while the amplitude of the average quadratic velocity varies greatly. The results are caused by the different interior acoustic excitations, and the distribution of the resonance peaks mainly reflects the natural modes of the structure at low frequencies. With the frequency increasing, the effect of the object on the structural response decreases gradually.

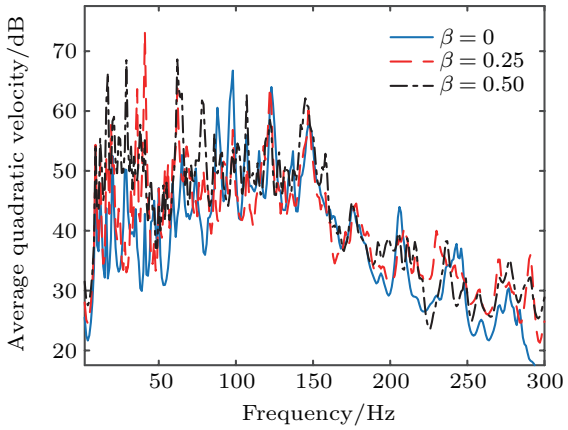


Fig. 9. (color online) Variations of average quadratic velocity with the frequency of the shell for different values of β.

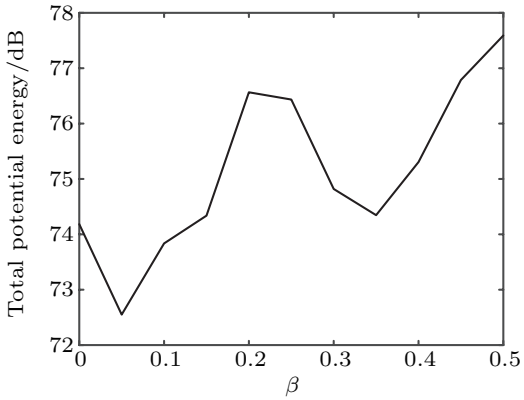


Fig. 10. Total average quadratic velocity of the shell below ring frequency.

In order to study the general trend of structural characteristics affected by the internal object occupation, the total kinetic energy of structural vibration is also analyzed below the ring frequency. Figure 10 shows that the change of the total average quadratic velocity is less than 6 dB.

3.4. Radiation analysis

In applications, radiated sound power is an important parameter in vibro-acoustic response prediction, which reflects the radiated energy of the structure excited by internal machinery. Like the case with average quadratic pressure inside the cylindrical shell, the first few resonant peaks of the radiated sound power are shifted to the low frequency with the object volume increasing in Fig. 11. Clearly, the phenomenon is caused by the change of internal acoustic field. It should be mentioned that compared with the scenario in Fig. 4, the volume occupation of the internal object cannot make a great contribution to the radiated sound power, because only a part of the sound energy can effectively pass through the shell into the external fluid.

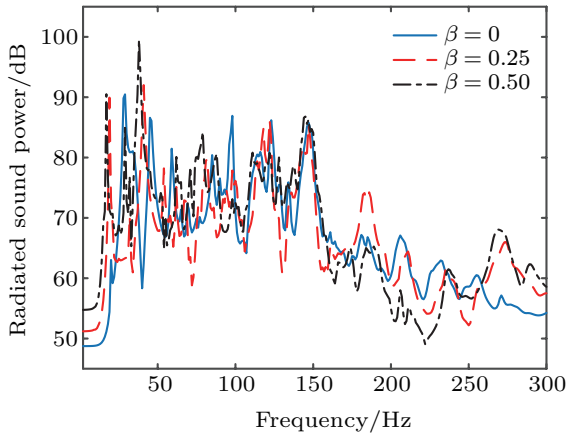


Fig. 11. (color online) Radiated sound power with different values of β.

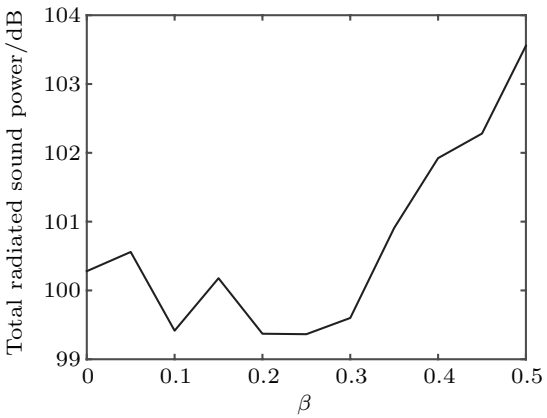


Fig. 12. Total radiated sound power below ring frequency.

The total sound power below ring frequency is given in Fig. 12, which describes the relationship between the general trend of the acoustic radiation and the object size. In the case of $\beta < 0.3$, the curve of total sound pressure varies gently within 1 dB. For $\beta > 0.3$, the total sound pressure appears to have an increasing trend, but the effect is still less than 4 dB. Consequently, the sound power radiated is much less affected by the object volume occupation than the interior acoustic field.

Further analysis is made to identify contributions of the object size to the sound radiation which can be expanded among modes with different circumferential orders in Figs. 13(a) and 13(b) for $n = 0$–7. It can be observed that the acoustic radiation has a strong influence on phenomena controlled by low circumferential order modes and a weak influence on those controlled by high circumferential order modes. The phenomena in Fig. 13 are mainly dominated by the $n = 1$ order.

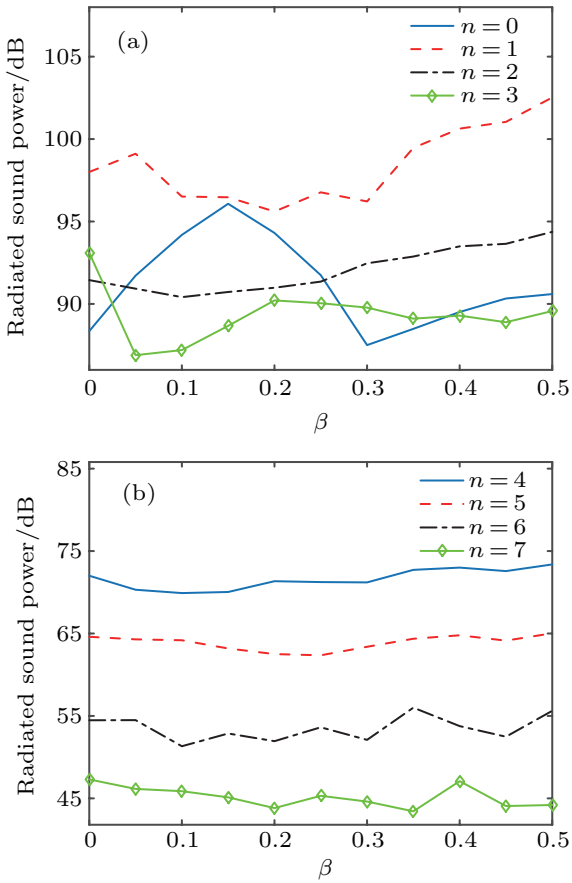


Fig. 13. (color online) Radiated sound powers of the shell with $n = 0$–3 (a) and $n = 4$–7 (b).

Far-field directivity is useful and instructive not only because it shows the spatial distribution of radiated acoustic energy, but also because it reflects the nature of the radiated acoustic energy which produces the radiation. Due to the sharp peaks and dips of the far-field pressure which varies with frequency, the results at a single frequency may not reflect the true nature of the radiated field. Figure 14 presents the far-field

directivity curves for the averaged pressure over different frequency bands. The results are evaluated at $r/R = 100$ and $z = L/2$, for a low-frequency broadband of $k_e = [0,\ 0.05]$, $[0,\ 0.1]$, and $[0,\ 0.2]$, respectively, with k_e being the wavenumber in the fluid outside the shell. The curves are symmetric with respect to the $\theta = [0,\ 180°]$ in the circumferential direction. Obviously, the radiation patterns for the case of $k_e = [0,\ 0.05]$ indicate that the radiated field is dominated by the $n = 0$ mode with some slight contribution from the $n = 1$ mode, causing a small distortion. By contrast with an empty shell, the existence of the object enhances the coupling between different modes, which leads to the increase of the contribution of the high-order modes in the low-frequency range, and eventually leading to the changes of the directivity of the far-field pressure. As frequency increases, the results cannot be described by any simple mode, and the effect of the object volume occupation gradually decreases. The results illustrate that the internal object volume occupation has a major contribution to acoustic radiation on the resonant peaks rather than radiated acoustic energy.

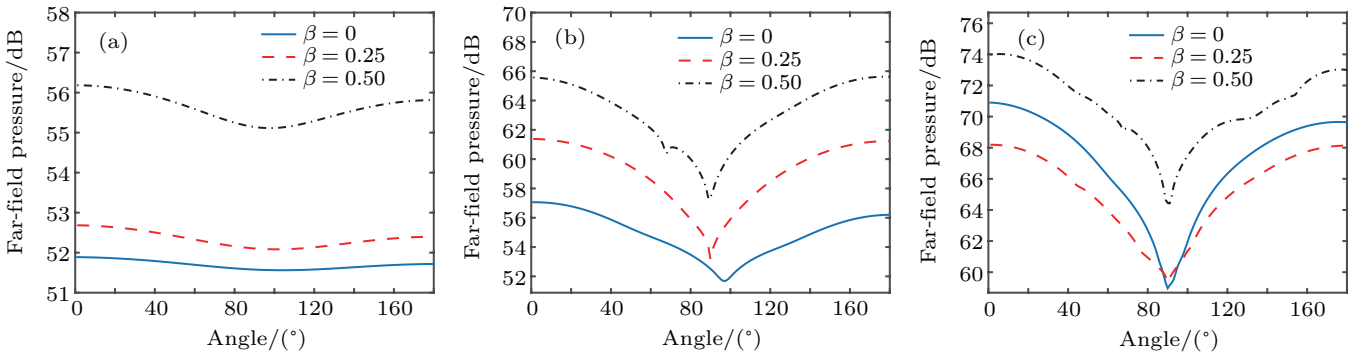


Fig. 14. (color online) Plots of far-field pressure versus angle at $k_0 = [0\ \ 0.05]$ (a), $k_0 = [0\ \ 0.1]$ (b), and $k_0 = [0\ \ 0.2]$ (c).

4. Conclusions

The structural-acoustic coupling characteristics of a submerged finite cylindrical shell with irregular-shaped acoustic enclosure are investigated. Due to the existence of an internal object, the sound transmission and radiation process involve a complex structural-acoustic coupling. Numerical simulations are conducted to determine the relationship between object size and shell behavior. The main conclusions can be drawn as follows.

The existence of an internal object changes the cavity from a regular- into an irregular-shaped enclosure. The pressure distribution inside the cavity is sensitive to geometrical changes. The internal object affects the resonance frequencies of the enclosure and corresponding mode shapes. The resonant frequencies of the first few natural modes shift to the low frequency as object volume increases. The relationship between resonant frequencies and spatial scale, which is generally applicable to regular cavities, is not always suitable for those with irregular shapes. Furthermore, irregularity can enhance the structural-acoustic coupling between different modes.

The influence of object volume on vibration is mainly reflected by the change in structure response in the low-frequency range, especially with respect to vibration strength. This phenomenon is evidently caused by the change of internal acoustic excitation. As frequency increases, the change in structural response decreased gradually for different object sizes. The change in the total average quadratic velocity is less than 6 dB below the ring frequency.

Unlike structural vibration, the contribution of the object volume occupation to sound radiation is mainly the distribution of resonance peaks, while the effect is non-significant on energy radiation. Given that only a part of the sound energy can effectively pass through the shell and into the external fluid, the sound radiation is less affected by object volume occupation than the interior acoustic field. In addition, object volume occupation enhances the directivity of far-field pressure in the low-frequency range.

References

[1] Dowell E H and Voss H M 1963 *AIAA J.* **1** 476
[2] Lyon R H and Voss H M 1963 *J. Acoust. Soc. Am.* **35** 1791
[3] Narayanan S and Shanbhag R L 1981 *J. Sound. Vib.* **78** 453
[4] Narayanan S and Shanbhag R L 1981 *J. Sound. Vib.* **77** 251
[5] Dowell E H, Gorman G F and Smith D A 1977 *J. Sound. Vib.* **52** 519
[6] James J H 1982 *Nasa Sti/recon Tech. Report N* **82** 5
[7] Fuller C R 1986 *J. Sound. Vib.* **109** 259
[8] Morfey C L 1971 *International Congress on Acoustic, Budapest-Proc.* 7th, 1971, Great Britain, Southamption, p. 221
[9] Joon H L and Kim J 2003 *Appl. Acoust.* **64** 611
[10] Laulagnet B and Guyader J L 1990 *J. Sound. Vib.* **138** 173
[11] Skelton E A 1991 *J. Sound. Vib.* **148** 243
[12] Jin G L, Yin J F, Wen J H and Wen X S 2016 *Acta Phys. Sin.* **65** 014305 (in Chinese)
[13] Pan A, Fan J and Zhuo L K 2012 *Acta Phys. Sin.* **61** 214301 (in Chinese)
[14] Cheng L and Nicolas J 1992 *J. Acoust. Soc. Am.* **91** 1504
[15] Cheng L 1994 *J. Sound. Vib.* **174** 641
[16] Guo Y P 1992 *J. Acoust. Soc. Am.* **91** 926
[17] Rebillard E, Laulagnet B and Guyader J L 1992 *Appl. Acoust.* **36** 87
[18] Guo Y P 1993 *J. Acoust. Soc.* **93** 1936
[19] Titovich A S and Andrew N 2015 *J. Sound. Vib.* **338** 134
[20] Missaoui J and Cheng L 1997 *J. Acoust. Soc. Am.* **101** 3313

[21] Anyunzoghe E and Cheng L 2002 *Appl. Acoust.* **63** 1233
[22] Li Y Y and Cheng L 2004 *J. Acoust. Soc. Am.* **116** 3312
[23] Missaoui J and Cheng L 1999 *J. Sound. Vib.* **226** 101
[24] Li D S, Cheng L and Gosselin C M 2002 *J. Sound. Vib.* **250** 903
[25] Achenbach J D, Bjarnason J and Igusa T 1992 *J. Vib. Acoust.* **114** 312
[26] Unruh J F and Dobosz S A 1988 *J. Vib. Acoust.* **110** 226
[27] Pan X, MacGillivray I, Tso Y and Peters H 2013 *Proc. Acoustics*, 2013, Australia, Victor Harbor, p. 1
[28] Pan X, Tso Y, Forrest J and Peters H 2014 I *Nter. Noise* 2014, Australia, Melbourne, p. 1
[29] Junger M C and Feit D 1972 *Sound, structures, and their interaction* (London: MIT Press)
[30] Stepanishen P R 1978 *J. Acoust. Soc. Am.* **63** 328
[31] Woo H and Shin Y S 2016 *J. Comput. Acoust.* **1** 24
[32] Stepanishen P R 1982 *J. Acoust. Soc. Am.* **71** 813
[33] Chen Y H, Jin G Y, Liu Z G and Feng Z M 2017 *Acta Acustica* **42** 694 (in Chinese)